Graphical Abstract

Sulfate limitation increases specific plasmid DNA yield and productivity in *E. coli* fed-batch processes

Mathias Gotsmy,Florian Strobl,Florian Weiß,Petra Gruber,Barbara Kraus,Juergen Mairhofer,Jürgen Zanghellini

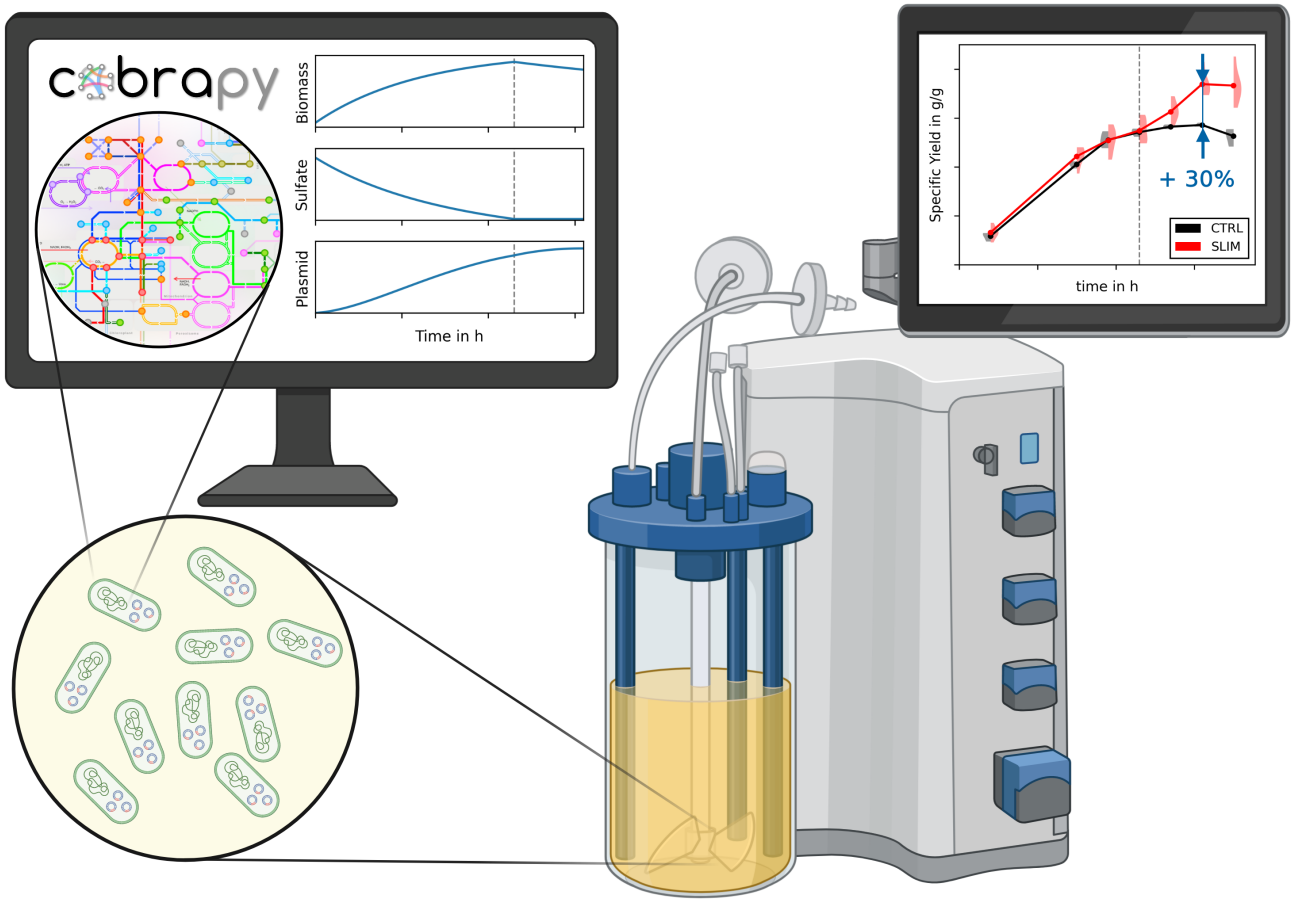

Highlights

Sulfate limitation increases specific plasmid DNA yield and productivity in *E. coli* fed-batch processes

Mathias Gotsmy,Florian Strobl,Florian Weiß,Petra Gruber,Barbara Kraus,Juergen Mairhofer,Jürgen Zanghellini

- Genome-scale metabolic models predict growth decoupling strategies.
- Sulfate limitation decouples cell growth from pDNA production.
- Sulfate limitation increases the specific supercoiled pDNA yield by 33 % and the volumetric productivity by 13 %.
- We propose that sulfate limitation improves the biosynthesis of over 25 % of naturally secreted products in *E. coli*.

Sulfate limitation increases specific plasmid DNA yield and productivity in *E. coli* fed-batch processes

Mathias Gotsmy[a,b], Florian Strobl[c], Florian Weiß[c], Petra Gruber[d], Barbara Kraus[d], Juergen Mairhofer[c] and Jürgen Zanghellini[a,*]

[a]*Department of Analytical Chemistry, University of Vienna, Vienna, 1090, Austria*
[b]*Doctorate School of Chemistry, University of Vienna, Vienna, 1090, Austria*
[c]*enGenes Biotech GmbH, Vienna, 1190, Austria*
[d]*Baxalta Innovations GmbH, A Part of Takeda Companies, Orth an der Donau, 2304, Austria*

ARTICLE INFO

Keywords:
growth decoupling
medium optimization
GSMM
FBA
dFBA
E. coli
plasmid production

ABSTRACT

Plasmid DNA (pDNA) is a key biotechnological product whose importance became apparent in the last years due to its role as a raw material in the messenger ribonucleic acid (mRNA) vaccine manufacturing process. In pharmaceutical production processes, cells need to grow in the defined medium in order to guarantee the highest standards of quality and repeatability. However, often these requirements result in low product titer, productivity, and yield.

In this study, we used constraint-based metabolic modeling to optimize the average volumetric productivity of pDNA production in a fed-batch process. We identified a set of 13 nutrients in the growth medium that are essential for cell growth but not for pDNA replication. When these nutrients are depleted in the medium, cell growth is stalled and pDNA production is increased, raising the specific and volumetric yield and productivity. To exploit this effect we designed a three-stage process (1. batch, 2. fed-batch with cell growth, 3. fed-batch without cell growth). The transition between stage 2 and 3 is induced by sulfate starvation. Its onset can be easily controlled via the initial concentration of sulfate in the medium.

We validated the decoupling behavior of sulfate and assessed pDNA quality attributes (supercoiled pDNA content) in *E. coli* with lab-scale bioreactor cultivations. The results showed an increase in supercoiled pDNA to biomass yield by 33 % and an increase of supercoiled pDNA volumetric productivity by 13 % upon limitation of sulfate.

In conclusion, even for routinely manufactured biotechnological products such as pDNA, simple changes in the growth medium can significantly improve the yield and quality.

Contents

1 Introduction **1**

2 Methods **3**
2.1 Metabolic Modeling 3
2.2 Validation Experiments 4

3 Results **6**
3.1 Key Objective 6
3.2 Identification of Decoupling Compounds . . 6
3.3 Optimal Sulfate Limited Processes 7
3.4 Sulfate Limitation Experiments 7

4 Discussion **9**

5 Conclusion **13**

A Supplementary Information **18**
A.1 Supplementary Tables 18
A.2 Supplementary Figures 21
A.3 Supplementary Notes 26

*Corresponding author
ORCID(s): 0000-0003-1333-4870 (M. Gotsmy); 0000-0002-2686-1971 (J. Mairhofer); 0000-0002-1964-2455 (J. Zanghellini)

1. Introduction

Plasmid DNA (pDNA) is an important product of the pharmaceutical industry being primarily used as vectors for the transfection of mammalian cells. For example, pDNA can be directly injected in the form of a DNA vaccine [1]. Moreover, it is an important raw material for the production of mRNA vaccines, for example against SARS-CoV-2 [2, 3]. Additionally, pDNA can be used as a vector for gene therapy [4]. Regardless of the application, high amounts and high quality of pDNA are needed and the optimization of its production is of health-economic interest as pDNA is a relevant driver of manufacturing costs.

Apart from solely maximizing the yield of pDNA, three prerequisites are required for the design of a pDNA production process. Firstly, pDNA can be present in an open circular (oc), linear (l), or covalently closed circular (ccc), i.e., supercoiled form. Generally, the ccc form is considered

more favorable for transfection of mammalian cells and, therefore, the fraction of supercoiling is of importance [5, 6]. Secondly, a loss of plasmid can be severely detrimental to the productivity during the fermentation process. Classically, this problem can be mitigated by the introduction of antibiotic resistance selection systems and the usage of antibiotic selection pressure during fermentation. However, these systems have several downsides. They, on the one hand, shift metabolic resources from the production of pDNA to the production of antibiotic resistance proteins [7]. On the other hand, special care has to be taken to remove residual antibiotics during pDNA purification and the absence thereof has to be validated. Therefore, several alternatives have been developed [8] although still not state-of-the-art yet for pDNA manufacturing. Thirdly, even though pDNA production in complex media generates higher yields, chemically defined media are preferred for the production of high-quality and safe pharmaceuticals [1].

Many strategies for the increase of pDNA production have been published with a large fraction using *E. coli* as production organism [9]. The methods range from the screening of favorable strains to metabolic engineering through knocking-in and -out of genes to antibiotic-free selection systems and other highly optimized production strains [9]. Most strategies for increasing pDNA production can be grouped into two conceptual approaches: (i) the reduction of cell growth; (ii) ensuring a constant supply of DNA precursor metabolites. The methods differ widely in the way one (or both) aims are achieved.

Early on researchers found that a low growth rate increases the specific productivity of pDNA [10]. To achieve this in batch fermentations Galindo et al. [11] designed a medium that releases glucose enzymatically and thus downregulates glucose uptake and subsequently growth. Alternatively, Soto et al. [12] developed *E. coli* strain VH33 by knocking-out the main uptake pathway of glucose to achieve the same result. With this method, they could increase the production to 40 mg L^{-1} pDNA compared to 17 mg L^{-1} of the wild type strain [12]. Moreover, an optimization strategy for microaerobic environments was devised where *E. coli* strain W3110 improved pDNA production in presence of a recombinant expression of the *Vitreoscilla* hemoglobin protein [13]. In a subsequent study, this strain was tested in batch fermentations with different oxygen transfer rates and they concluded that as oxygen was depleted the growth rate decreased and the production of pDNA increased [14].

A strategy to ensure a constant supply of DNA precursor metabolites is, for example, the knocking-out of pyruvate kinase which forces metabolization of glucose over the pentose phosphate pathway [7, 15, 16]. Other methods utilize stoichiometric models to optimize the growth medium [17]. These authors concluded that the addition of the nucleosides adenosine, guanosine, cytidine, and thymidine as well as several amino acids can significantly improve pDNA production (60 mg L^{-1} in a batch fermentation). Martins et al. [18] optimized the growth medium for the high producer strain VH33 and concluded that the presence of aromatic amino acids (phenylalanine, tryptophan, tyrosine) is advantageous for redirecting molecules to the nucleotide synthesis pathways. Additionally, the effect of the amount and type of nitrogen source in the growth medium has been investigated on the production of pDNA to 213 mg L^{-1} [19]. Also, economical aspects of the medium design have been discussed [20].

Further potential for optimization is the pDNA itself. For example, reducing the size of the pDNA has been linked to higher volumetric yields [21]. However, a reduction might not always be possible, especially for therapeutic applications, where plasmid sizes are typically large (> 6 kb) [22]. Moreover, the pDNA yield of a process is highly dependent on the origin of replication. Currently, most plasmids carry a high copy number pUC origin of replication that allows up to 700 pDNA copies per cell [1]. Other approaches involved microaerobically induced [23] or heat-induced origins of replication that increase the plasmid copy number at higher temperatures than 37 °C [24, 25]. However, higher temperatures come with physiological trade-offs and, therefore, the amplitude and timing of heat induction are of importance [26].

Recently also other production organisms were proposed, e.g. *Lactococcus lactis*. Contrary to *E. coli*, *L. lactis* is generally regarded as safe (GRAS) and thus simplifies the downstream processing [27, 28].

Here, we design a three-stage bioprocess, where cellular growth and pDNA production are decoupled. We use constraint-based modeling to (i) identify medium components that induce the switching and (ii) determine the optimal time point for switching between the phases such that the average volumetric productivity is maximized.

2. Methods

2.1. Metabolic Modeling

All models and code used for the creation, simulation, and analysis of these models are available at https://github.com/Gotsmy/slim.

2.1.1. Model Creation

For our analysis, we used *i*ML1515 [29], a genome-scale metabolic model of *Escherichia coli* strain K-12 substrain MG1655. All model modifications and simulations were performed in Python 3.10 using the CobraPy package [30].

To simulate plasmid production, an 8 base pair (bp) dummy pDNA metabolite with 50 % GC content was added to the model. Subsequently, we added a pDNA production reaction, corresponding to the dummy plasmid's stoichiometry. pDNA polymerization cost was estimated to 1.36 mol adenosine triphosphate (ATP) per mol dNTP [7, 31]. Additionally, a pDNA sink reaction was introduced to make fluxes through the pDNA synthesis reaction feasible. An SBML version of the used model is available at https://github.com/Gotsmy/slim/tree/main/models.

Although 8 bp is an unrealistically small size for a real pDNA molecule, we emphasize that the actual length of the plasmid does not change the relative underlying stoichiometry. The reason we chose a small dummy plasmid is that it already has a molecular weight of approximately 4943.15 g mol^{-1}. If we included a multiple kbp sized plasmid into the model, we would have risked that its large molecular weight lead to numerical instabilities during simulation [32]. However, all results are shown in gram pDNA, therefore, the exact length of the dummy plasmid does not change the values.

2.1.2. Identification of Decoupling Compounds

Initially, we performed a parsimonious flux balance analysis (pFBA) [33] with biomass growth as objective. The maximal glucose uptake rate was set to 10 mmol g^{-1} h^{-1} and a non-growth associated maintenance requirement was set to 6.86 mmol ATP g^{-1} h^{-1} [29]. Exchange reactions with non-zero fluxes were used for the definition of the minimal medium. All exchange reactions that were not present in the minimal medium, except for H_2O and H^+, were turned off. To investigate the differences in uptake fluxes, an additional pFBA was performed with pDNA as the objective.

Next, we selected each of the minimal medium components and set the maximum exchange flux bound for this metabolite to 5, 25, 50, 75, and 100 % of the flux during biomass growth. For each value, a production envelope (pDNA synthesis as a function of growth) was calculated. Decoupling medium components were identified as metabolites which, as their uptake flux decreased, the maximum pDNA synthesis potential increased at a maximum biomass growth.

2.1.3. Process Simulation

We used dynamic flux balance analysis (dFBA) [34] to simulate the time evolution of the fed-batch processes. Only the feed phase was simulated (stage 2 and 3 in Figure 1) as the batch remained unchanged. At every integration step, a lexicographic flux balance analysis (FBA), where all fluxes of interest were consecutively optimized, was performed [35]. The list of objectives is given in Table 1. The non-growth associated maintenance was kept at a constant value as before. We used SciPy's `solve_ivp` function for numerical integration [36].

Sulfate concentration, $C_{SO_4^{2-}}(t)$, in the medium was tracked as its depletion coincides with the metabolic switch from biomass growth to production. Due to a lack of knowledge, no uptake kinetics of sulfate were simulated. Practically, this meant that the sulfate uptake was calculated from the biomass stoichiometry and growth rate. The exchange reaction bounds were left unconstrained when $C_{SO_4^{2-}}(t) > 0$ and were blocked when $C_{SO_4^{2-}}(t) \leq 0$.

High copy number origin of replication plasmids typically replicate during the growth phase as they high-jack genomic DNA synthesis pathways. Therefore, we set a lower bound, $q^{\mu}_{\text{pDNA}} = 4.9\,\text{mg}\,\text{g}^{-1}\,\text{h}^{-1}$, for the pDNA synthesis reaction. Moreover, it is unrealistic to assume that all available glucose is channeled towards pDNA production during the SO_4^{2-} starvation. Therefore, we set an upper bound to the synthesis reaction. Since its actual value was unknown, we tested several levels ranging from $q^{*}_{\text{pDNA}} = 4.9$ to $24.7\,\text{mg}\,\text{g}^{-1}\,\text{h}^{-1}$. Throughout this manuscript, that ratio of upper to lower bound of the pDNA synthesis reaction is referred to as

$$\kappa_{\text{pDNA}} = q^{*}_{\text{pDNA}} / q^{\mu}_{\text{pDNA}}. \tag{1}$$

We simulated 41 equidistant levels of $\kappa_{\text{pDNA}} \in [1, 5]$. Because of the implementation of the dFBA, the lower and upper bounds of the synthesis reaction can be interpreted as

Table 1
Lexicographic objectives for dFBA. The order of optimization was top to bottom.

	Objective
max	biomass production
min	sulfate uptake
max	pDNA production

the pDNA synthesis fluxes during the growth and SO_4^{2-} starvation phase, respectively. We assumed negligible changes in overall biomass composition due to pDNA synthesis, which solely derives from external carbon sources.

To compare pDNA production processes, we calculated two performance indicators: the specific yield

$$Y_{\text{pDNA/biomass}}(t) := C_{\text{pDNA}}(t)/C_{\text{biomass}}(t), \tag{2}$$

and the average volumetric productivity

$$p_{\text{pDNA}}(t) := \frac{C_{\text{pDNA}}(t) - C_{\text{pDNA}}(0)}{t - t_0}. \tag{3}$$

Here, $t_0 = 0\,\text{h}$ indicates the start of feeding (see Figure 1). With our parameters, see Table S1, (3) simplifies to

$$p_{\text{pDNA}}(t) = C_{\text{pDNA}}(t)/t.$$

A schematic of a three-stage growth-decoupled fed-batch process is shown in Figure 1. Initial conditions (at the start of the feed phase) resembled realistic values from the end of a batch process in a small bioreactor (Table S1). Strategies with a linear (i.e. constant) and an exponential feeding rate,

$$r^{\text{feed}} = \begin{cases} r_{\text{lin}}^{\text{feed}}, & \text{(4a)} \\ \mu C_{\text{biomass}}(0)V(0)Y_{\text{feed/biomass}} \exp(\mu t), & \text{(4b)} \end{cases}$$

respectively, were tested. The specific glucose uptake rate was set to

$$q_{\text{glucose}}(t) = \frac{r^{\text{feed}} C_{\text{glucose}}^{\text{feed}}}{C_{\text{biomass}}(t)V(t)} \tag{5}$$

to ensure $C_{\text{glucose}}(t) = 0$ throughout the (non-starved) fed-batch phase (stage 2, Figure 1). Here, $C_{\text{glucose}}^{\text{feed}}$ denotes the glucose concentration in the feed medium.

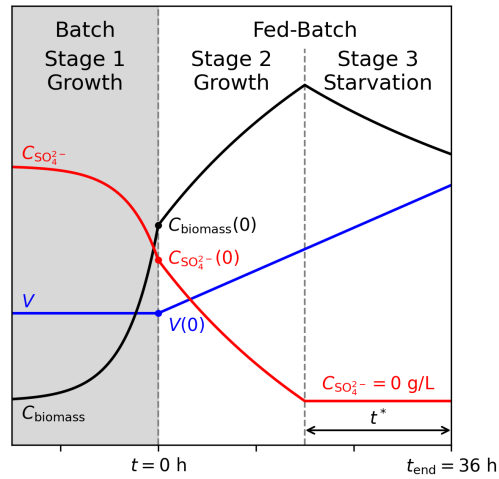

Figure 1: Schematic of a three-stage growth-decoupled fed-batch pDNA production process (1. batch, 2. fed-batch with cell growth, 3. fed-batch without cell growth). Size of the variables and length of the stages are not to scale. As the batch process was kept unchanged, it was not included in the fed-batch optimization simulations. Instead, the simulation starts at the beginning of the feed ($t = 0\,\text{h}$) with realistic values for the process variables at batch end (Table S1).

The dFBA simulation terminated once the maximal volume of 1 L was reached (i.e. after 35.2 and 36.0 h in exponential and linear fed-batch, respectively). The initial sulfate concentration in the medium at the start of feed was varied in 301 equidistant steps to search for a productivity optimum. We assumed that sulfate was present in the medium at the start of the feed, while the feed medium was sulfate-free.

2.1.4. Identifying Alternative Targets

We screened 307 products with existing exchange reactions in *i*ML1515 [29] by performing lexicographic FBA (analogous to Table 1) with and without sulfate in the growth medium. Bioproducts for which the calculated synthesis rate improved during sulfatelimitation were identified as potential products benefiting from a sulfate limited process design.

2.2. Validation Experiments

2.2.1. Upstream Process

All experiments were conducted with proline auxotroph *E. coli* K-12 strain JM108 [37], which previously had been used for pDNA production [8]. The cells were transformed with a plasmid of 12.0 kbp length and 53 % GC content containing a pUC origin of replication and a kanamycin

resistance gene. However, no kanamycin was added throughout the production process as U.S. Food and Drug Administration (FDA) and European Medicines Agency (EMA) recommend to avoid the use of antibiotics [1].

For fed-batch fermentations, *E. coli* JM108 were grown in a 1.8 L (1.0 L net volume, 0.5 L batch volume) computer-controlled bioreactor (DASGIP parallel bioreactor system, Eppendorf AG, Germany). The bioreactor was equipped with a pH probe and an optical dissolved oxygen probe (Hamilton Bonaduz AG, Switzerland). The pH was maintained at 7.0 ± 0.1 by addition of 12.5 % ammonia solution; the temperature was maintained at 37.0 ± 0.5 °C. The dissolved oxygen (O_2) level was stabilized above 30 % saturation by controlling the stirrer speed, aeration rate, and gassing composition. Foaming was suppressed by the addition of 2 mL 1:10 diluted Struktol J673A antifoam suspension (Schill+Seilacher, Germany) to the batch medium and by the automatic addition of 1:10 diluted Struktol J673A controlled by a conductivity-operated level sensor. For the inoculation of the bioreactor, a seed culture was used (25 mL batch medium inoculated with 250 µL master cell bank in 250 mL baffled glass flasks at 37 °C with shaking at 180 rpm). The seed culture was incubated until a final OD_{600} of 2-4 was reached and a defined volume was transferred aseptically to the bioreactor to result in an initial OD_{600} of 0.015.

The fermentation process was designed for a final amount of 50 g cell dry mass (CDM) of which 1.51 g was obtained in a batch volume of 500 mL and 48.5 g during the feed phase via the addition of another 500 mL of feed medium. The amount of glucose for the specific medium was calculated based on a yield coefficient ($Y_{\text{biomass/glucose}}$) of 0.303 g g^{-1} and added as $C_6H_{12}O_6 \cdot H_2O$. For media preparation, all chemicals were purchased from Carl Roth GmbH (Germany) unless otherwise stated. Two different media compositions were compared regarding specific pDNA productivity: one with a limited sulfur source (SO_4^{2-} limitation) and one without a limited sulfur source (control). Feeding was initiated when the culture in the batch medium entered the stationary phase. A fed-batch regime with a linear substrate feed (0.26 g min^{-1} respectively 13.91 mL h^{-1}) was used for 35 h (approximately five generations). During SO_4^{2-} limitation fermentations, the simulations predicted that the provided sulfur was completely consumed at 23 h after feed start. The batch and fed-batch medium components are given in Table S2. The cultivations of SO_4^{2-} limitation and control were conducted in six and three replicates, respectively.

2.2.2. Analysis

For off-line analysis (OD_{600}, CDM, pDNA product), the bioreactor was sampled during the fed-batch phase. The OD_{600} was measured using an Ultrospec 500 pro Spectrophotometer (Amersham Biosciences, UK), diluting the samples with phosphate-buffered saline to achieve the linear range of measurement. For the determination of CDM, 1 mL of cell suspension was transferred to pre-weighed 2.0 mL reaction tubes and centrifuged for 10 min at 16.100 rcf and 4 °C with an Eppendorf 5415 R centrifuge. The supernatant was transferred to another reaction tube and stored at −20 °C for further analysis. As a washing step, the cell pellet was resuspended in 1.8 mL RO-H_2O, centrifuged, and the supernatant discarded. Afterwards, the pellet was resuspended in 1.8 mL RO-H_2O and finally dried at 105 °C for 24 h. The reaction tubes with the dried biomass were cooled to room temperature in a desiccator before re-weighing.

For pDNA product analysis, the sampling volume of the cell suspension, corresponding to 20 mg CDM, was estimated via direct measurement of the OD_{600}. The calculated amount was transferred to 2.0 mL reaction tubes and centrifuged at 16.100 rcf and 4 °C for 10 min. The supernatant was discarded, and the cell pellets were stored at −20 °C.

The content of pDNA in ccc-conformation was determined using AIEX-HPLC (CIMac™ pDNA-0.3 Analytical Column, 1.4 µL; BIA Separations d.o.o., Slovenia). The column separated open circular, linear, and supercoiled pDNA fractions into distinct peaks. Quantification was achieved using a calibration curve based on peak areas obtained from purified pDNA samples. For HPLC analysis cell disintegration was performed by an alkaline lysis method [38]. The obtained lysate was directly analyzed by HPLC (Agilent 1100 with a quaternary pump and diode-array detector (DAD)). Values derived from three biological replicates have a coefficient of variation lower than 10 %.

The average volumetric productivity ($p_{\text{pDNA}}(t)$) and the average specific yield ($Y_{\text{pDNA/biomass}}(t)$) were calculated as given in Equations (3) and (2), respectively. The time-dependent pDNA synthesis rate ($q_{\text{pDNA}}(t)$) was estimated via the `finitediff` Python package [39, 40].

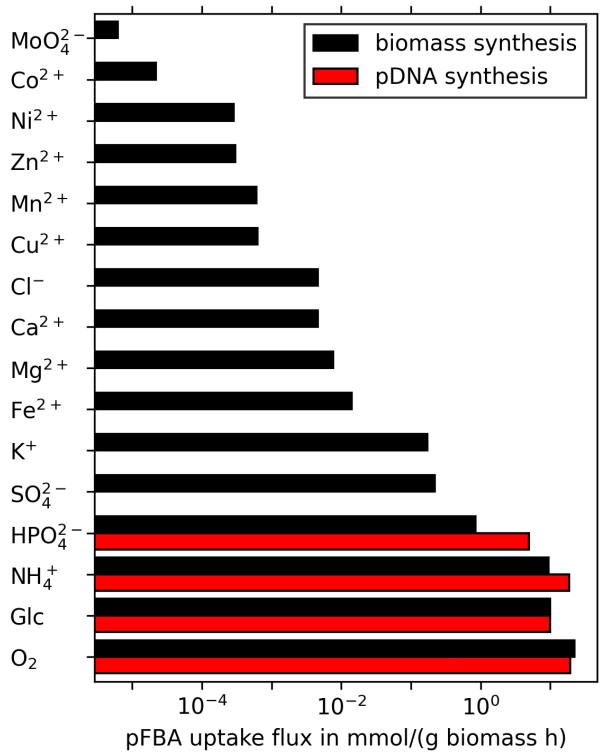

Figure 2: pFBA uptake flux rates for all minimal medium components. Black bars represent fluxes for optimization of biomass synthesis, red bars represent fluxes of pDNA synthesis.

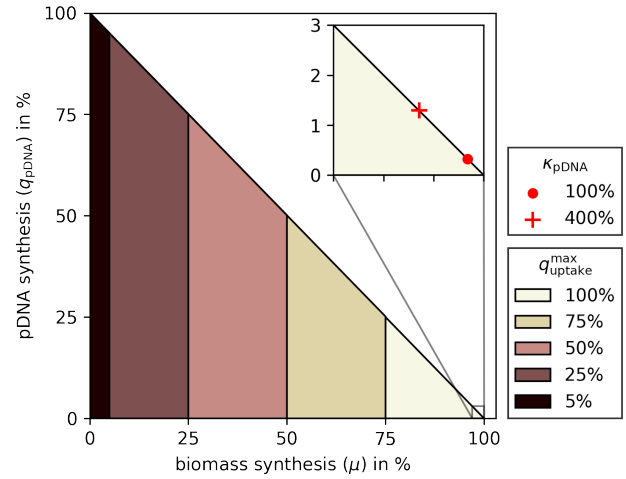

Figure 3: Normalized pDNA production envelopes for different maximal uptake rates of (a single) decoupling nutrient. Ca^{2+}, Cl^-, Co^{2+}, Cu^{2+}, Fe^{2+}, K^+, Mg^{2+}, Mn^{2+}, MoO_4^{2-}, Ni^{2+}, SO_4^{2-}, and Zn^{2+} all result in identical sets of production envelopes. Note that all production envelopes include the line segment from (0|0) to (0|100). The inset shows the extreme points of a production envelope with a realistic pDNA production rate during biomass growth (red circle) and a potential 4-fold pDNA production rate increase (red cross).

3. Results

3.1. Key Objective

We aim to design an efficient three-stage fed-batch process (Figure 1) for pDNA production in *E. coli*, where cellular growth and pDNA production are separated.

In the following, we will

(i) use constraint-based modeling to identify medium components that enable switching from growth to production phase;

(ii) determine optimal switching time points to maximize the average productivity in a fed-batch fermentation; and

(iii) experimentally validate the computed strategies in a linear fed-batch process.

3.2. Identification of Decoupling Compounds

First, we used pFBA to compute a minimal set of uptake rates in the genome-scale metabolic model *i*ML1515 [29] supporting maximal aerobic growth of *E. coli* with glucose as carbon source. Similarly, we computed uptake rates for maximal pDNA production using the same constraints (Figure 2). All calculated uptake rates are inflexible in the optima, except for Fe^{2+} and O_2. Their uptake can be further increased by conversion to and excretion of Fe^{3+} and H_2O. In contrast to biomass synthesis, pDNA production requires only glucose, O_2, NH_4^+, and HPO_4^{2-}, but no further nutrients. Therefore, we conclude that these remaining nutrients could potentially be used as decoupling agents separating pDNA synthesis from growth.

Next, for each decoupling nutrient, we restricted its uptake between zero and 100 % of its rate at maximum growth and computed the corresponding pDNA production envelopes as a function of growth (Figure 3). All twelve decoupling nutrients result in identical sets of production envelopes, which mirrors the fact that each decoupling nutrient is essential for growth but not required for pDNA production. Note that the one-to-one trade-off between biomass production and pDNA synthesis, i.e., the upper limit of the production envelope, is a straight line between the points (0|100) and (100|0).

Realistically, pDNA production rates are significantly less than the theoretical value of 100 % in Figure 3. Therefore, in the inset of the same figure, the red markers illustrate the extreme points of more reasonable production envelopes.

For example, the red circle (i.e., $\kappa_{\mathrm{pDNA}} = 100\,\%$) illustrates average rates of pDNA production during cell growth. Even when the decoupling would lead to a boost by a factor of $\kappa_{\mathrm{pDNA}} = 4$ (red cross), the resulting pDNA production flux would be only 1.3 % of the theoretical maximum.

In the following, we focus on the impact of the six bulk non-metal elements (sulfur, phosphorus, oxygen, nitrogen, carbon, and hydrogen) that typically make up 97 % ($\mathrm{g\,g^{-1}}$) of the elemental biomass composition [41]. Moreover, except for potassium (and sulfate), all other predicted decoupling nutrients (iron, magnesium, calcium, chlorine, copper, manganese, zinc, nickel, cobalt, and molybdenum) are taken up at minute rates ($< 15\,\mathrm{\mu mol\,g^{-1}\,h^{-1}}$, Figure 2). Thus, exactly dosing their concentrations for limitation may be challenging in a bio-process. This leaves sulfate as the only predicted decoupling nutrient in a glucose-minimal medium.

3.3. Optimal Sulfate Limited Processes

Decoupling production from growth during a bio-process raises the question of timing: when to best switch from growth to production phase to maximize performance.

In the following, we used dFBA [34] to track the time-dependent concentrations $C_i(t)$ of biomass, pDNA, glucose, and sulfate and determine the optimal initial sulfate concentration, $C_{SO_4^{2-}}(0)$, that maximize the average volumetric productivity

$$\max_{C_{SO_4^{2-}}(0)} p_{\mathrm{pDNA}}\left(t_{\mathrm{end}}, C_{SO_4^{2-}}(0)\right) \tag{6}$$

in a fed-batch process. Here t_{end} denotes the end of the bio-process, which terminates when the maximal volumetric capacity of the reactor is reached. Our simulations assume that pDNA production occurs (i) at a constant rate $q^*_{\mathrm{pDNA}} = \kappa_{\mathrm{pDNA}} q^{\mu}_{\mathrm{pDNA}}$ during the sulfate starvation phase; (ii) at q^{μ}_{pDNA} during the growth phase.

We simulated sulfate limited fed-batch processes with a linear feed as sketched in Figure 1 using the values listed in Table S1. In all simulations the feed rate was constant. Thus, the process length is always 36 h. Subsequently, we analyzed the impact of the length of the pDNA production phase (induced by sulfate starvation during the feed phase, i.e. stage 3 in Figure 1) on the average volumetric productivity. An analogous analysis for a sulfate limited batch fermentation can be found in the Supplementary Notes A.3.1.

We observed distinct maxima in the average volumetric productivity of a linear fed-batch when $\kappa_{\mathrm{pDNA}} > 1$ (red dotted line, Figure 4A). Maxima occur at much longer starvation times compared to batch processes ($t^* = 19\,\mathrm{h}$ versus 2.5 h at $\kappa_{\mathrm{pDNA}} = 4$, Figure S1). Even compared to an equivalent exponential fed-batch, the optimal starvation is longer in a linear than in an exponential fed-batch process (Figure S2). For instance, at $\kappa_{\mathrm{pDNA}} = 1.5$ a linear fed-batch process achieves an optimal $p_{\mathrm{pDNA}} = 0.18\,\mathrm{g\,L^{-1}\,h^{-1}}$ at $t^* = 12\,\mathrm{h}$, while an equivalent exponential fed-batch process reaches its optimum $p_{\mathrm{pDNA}} = 0.096\,\mathrm{g\,L^{-1}\,h^{-1}}$ at $t^* = 3.3\,\mathrm{h}$. Within our modelling assumptions, a linear fed-batch, even without starvation, outperforms an equivalent exponential fed-batch with (optimal) sulfate starvation as long as $\kappa_{\mathrm{pDNA}} \leq 3.5$.

Typically, growth-decoupled processes suffer from a substantially decreasing (glucose) uptake rate during the production phase [42, 43]. Thus, our assumption of keeping an elevated q^*_{pDNA} constant over several hours may be unrealistic. Therefore, we investigated how the productivity optima change when the maximal feasible starvation length (t^*_{max}) is bounded. Yet, even in such cases, sulfate limited fed-batches perform better than standard processes without starvation (Figure S3).

3.4. Sulfate Limitation Experiments

The preceding analysis suggested that a three-stage fed-batch process with sulfate starvation will deliver superior pDNA production performances compared to a conventional, non-starved fed-batch process. To confirm this, we set up a linear fed-batch process with *E. coli* JM108 as host (see Section 2.2 for details). Based on small molecule production rates during sulfate starvation [43, 44], we assumed a $\kappa_{\mathrm{pDNA}} = 2$ and consequently predicted $t^* = 13\,\mathrm{h}$. Thus, we computed the initial SO_4^{2-} concentration to be $3.8\,\mathrm{g\,L^{-1}}$ such that sulfate starvation occurs after 23 h in a 36 h bio-process.

Figure 5 highlights the feasibility of sulfate starvation (indicated as SLIM) to boost pDNA production in a (linear) fed-batch. Panel A illustrates the growth arrest due to sulfate starvation (compare the diverging lines to the right of the dashed line). Due to dilution, the biomass concentration (red) decreases if cells no longer grow. Yet, pDNA concentration keeps rising – even faster than in the unstarved control (compare red SLIM with black CTRL in panel B). Consequently, the specific pDNA yield rises too (panel C) reaching a maximum of $0.074\,\mathrm{g\,g^{-1}}$ after 31 h, which corresponds to an improvement of 29 % compared to control ($p = 0.0005$, Table S3).

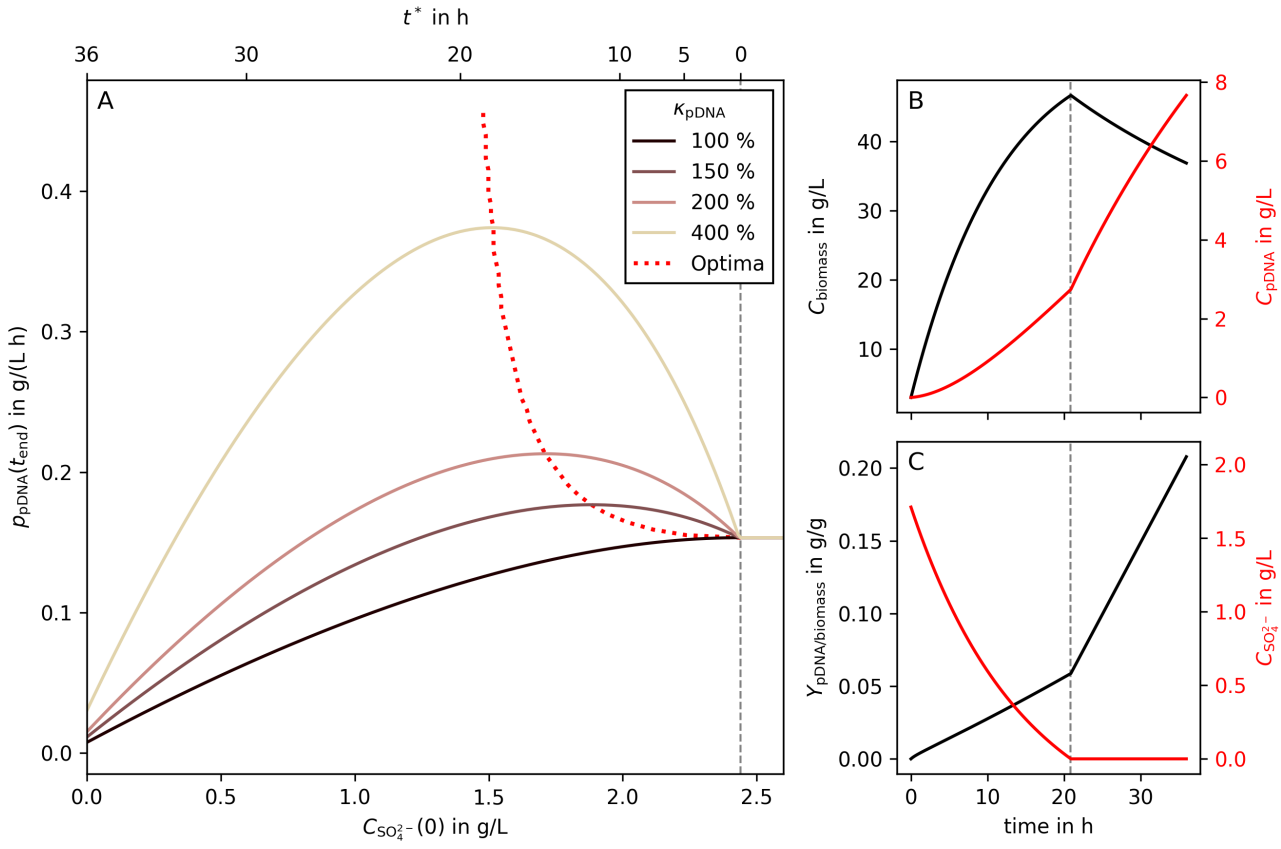

Figure 4: Predicted optimal timing in a SO_4^{2-} limited linear fed-batch process. Panel **A** shows average volumetric productivities of pDNA production ($g\,L^{-1}\,h^{-1}$) as a function of the initial SO_4^{2-} concentration in a linear fed-batch process. The full line represents different levels of increased pDNA production during starvation as percentages of pDNA production rate during biomass growth (κ_{pDNA}). The dotted line indicates the location of the optima for κ_{pDNA} between 100 and 500 %. The second X-axis of panel **A** (top) illustrates the length of the sulfate starved process phase (t^*). For all modeled linear fed-batch processes, right of the gray dashed line, no SO_4^{2-} limitation occurred. Panels **B** and **C** show the process curves of metabolites of interest in the optimal process for $\kappa_{pDNA} = 200\,\%$. The gray dashed lines indicate the switching time point between the growth and production phases.

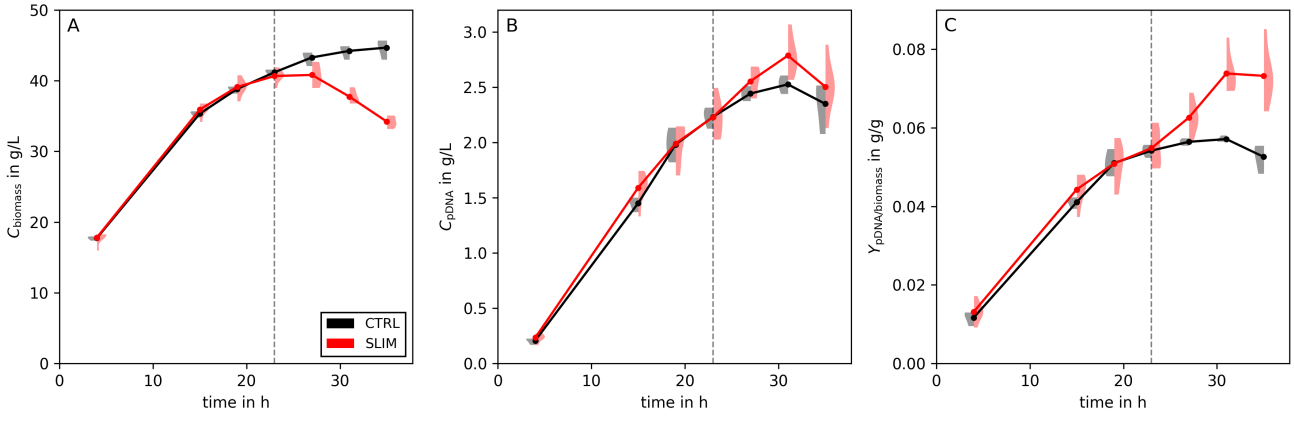

Figure 5: Experimental results of sulfate limitation. Panel **A** illustrates the biomass concentration, panel **B** the concentration of produced pDNA, and panel **C** the pDNA to biomass yield. The violins are calculated from triplicates of the control (i.e., no SO_4^{2-} limitation, CTRL, black) and six replicates of sulfate limited processes (SLIM, red) are shown. The full lines and points are calculated from the mean of the replicates. The gray dashed line represents the estimated time of the switch from biomass growth to pDNA production (projected at 23 h).

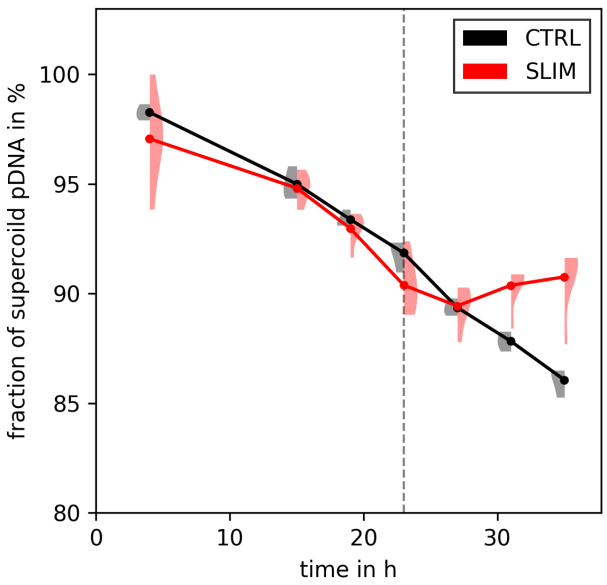

Figure 6: Fraction of supercoiled (ccc) pDNA over time for SO_4^{2-} limited (SLIM, red) and control (CTRL, black) process. Experimental replicates are shown as violins, full lines and markers represent their means.

Moreover, we compared the fraction of supercoiled pDNA between the SO_4^{2-} limited and control processes (Figure 6). Up to 27 h after induction, there were no noticeable differences. After this point, the SO_4^{2-} limited process maintained a higher fraction of supercoiled pDNA (+3%, $p = 0.0019$, Table S3), resulting in a 33 % ($p = 0.0001$) increase in the specific yield of supercoiled pDNA.

Beyond 31 h pDNA concentration and specific yield decrease in both the SO_4^{2-} limited and the control process.

Next to the specific yield, also the average volumetric productivity increases by 10 % at 31 h ($p = 0.0243$, Figure 7A and Table S3). If only the pharmacologically relevant supercoild fraction of pDNA is considered, the productivity increases by 13 % ($p = 0.0052$, Table S3).

To further investigate the experimental results, we computed the specific productivities in the sulfate limited and control fermentations (Figure 7B). In both bio-processes q_{pDNA} decreases with time which is in contrast to our modeling assumptions.

Finally, we compared the specific and volumetric yield achieved by the experiments in this study (at $t = 31$ h) to published values. Table 2 shows that in terms of volumetric and specific yield the pDNA production strategy for our control values is already one of the best we could find, and with SO_4^{2-} limitation it performs better than all other published methods of our knowledge. Due to the extraordinary pDNA size in this study, the plasmid copy number is just above average. However, compared to the control, the plasmid copy number of the sulfate limited process increases by 29 %.

4. Discussion

We aimed to improve pDNA productivity by designing a three-stage fed-batch process that separates cellular growth and production. Growth-decoupled processes are common design choices to enhance volumetric productivity in biochemical and biopharmaceutical production processes [43–46]. Especially with the advent of dynamic control in metabolic engineering that allows switching back and forth between metabolic growth and production phenotypes, interest in such (multi-stage) process designs has strongly grown [47]. While algorithms like MoVE [48] exist to identify intracellular metabolic switches, our focus here was on easily implementable medium modifications to induce these switches.

In this study, we identified twelve possible decoupling components (SO_4^{2-}, K^+, Ca^{2+}, Cl^-, and compounds of trace elements) for the production of pDNA (Figure 2 and 3). All of them enable and regulate key functions in life [49]. Although trace elements act primarily as catalysts in enzyme systems, some of them, like copper and iron, play vital roles in energy metabolism [50]. However, we specifically selected SO_4^{2-} for further investigations because: (i) Sulfate is one of the six most prevalent elements in living organisms [41], which makes it comparably easy to measure and consequently determine the onset of starvation; (ii) Sulfate, in contrast to the other decoupling compounds, has a dedicated metabolic function that is well captured in the used genome-scale metabolic reconstruction *i*ML1515 of *E. coli*. [29]; (iii) Sulfate itself neither has a catalytic function nor a role in energy metabolism [51].

We simulated a three-stage fed-batch process where the transition from growth to production is triggered by the onset of sulfate starvation. Our computational model is based on two assumptions: (i) In each phase the specific pDNA production rate is constant; (ii) pDNA productivity increases upon starvation, i.e. $\kappa_{\text{pDNA}} = q^*_{\text{pDNA}}/q^{\mu}_{\text{pDNA}} > 1$. The latter aligns with experimental results of Masuda et al. [43], who reported a value of $\kappa_{\text{mevalonate}} = 1.16$ for mevalonate production during sulfate starvation.

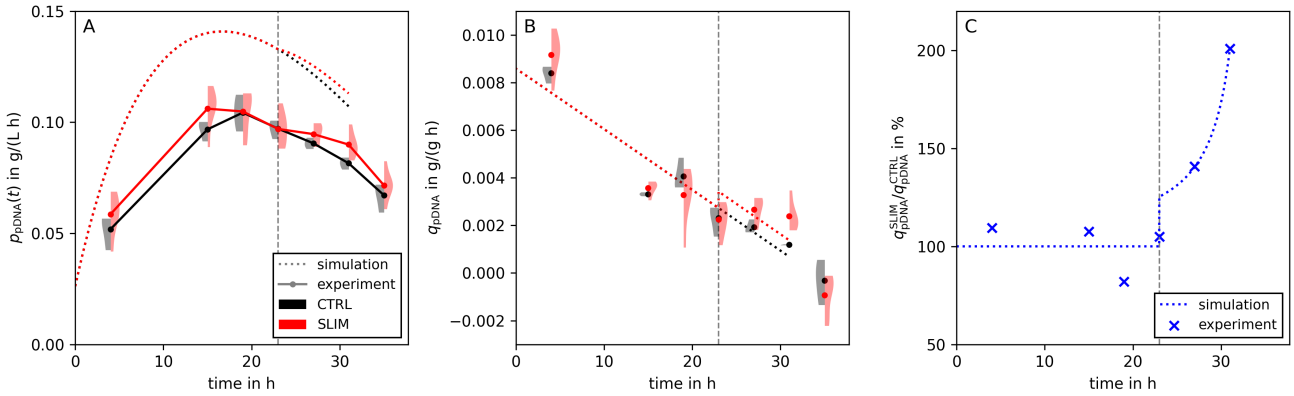

Figure 7: Calculated experimental rates and comparison to the simulation. Panel **A** illustrates the average volumetric productivity and panel **B** the pDNA production fluxes of control and SO_4^{2-} limited process (black CTRL and red SLIM, respectively). Panel **C** shows the ratio of q^{SLIM}_{pDNA} and q^{CTRL}_{pDNA} (blue). Experimental replicates are shown as markers, dotted lines are calculated from simulations. To adjust the simulations to the rates obtained in the experiments, a linearly decreasing q^{CTRL}_{pDNA} was fitted to experimental control data (black dotted line, panel **B**). Moreover, we fitted a parallel q^{SLIM}_{pDNA} (red dotted line, panel **B**) to conform to the experimental flux ratio (panel **C**). The vertical gray dashed line represents the estimated time of switching from biomass growth to pDNA production (projected at 23 h).

In our experiments, we observed a decrease in the specific pDNA production for both the control and SO_4^{2-} limited process (Figure 7B), challenging our assumption of a constant specific pDNA production rate. Investigating why q_{pDNA} decreases throughout the process will be the scope of further work. However, we implemented a time-dependent q_{pDNA} in additional simulations which demonstrate that the assumption of constant q_{pDNA} is not necessary for process improvements by SO_4^{2-} limitation (dotted lines in Figure 7 and S6) Even the optimal switching time changes by less than 1 h (Figure S7). Sulfate starvation always increases pDNA production, provided that $\kappa_{pDNA} > 1$, regardless of the process (batch, exponential or linear fed-batch). In fact, our data consistently shows higher specific pDNA production rates during starvation compared to control (Figure 7C). This trend reinforces and validates our core assumption of $\kappa_{pDNA} > 1$ where the length of starvation required to maximize volumetric productivity strongly depends on its exact value.

Maintaining high κ_{pDNA} during sulfate starvation is a key requirement of our design. Our predictions are based on continuously elevated levels of pDNA productivity throughout starvation. For long starvation phases, this assumption may not be feasible [52]. However, Figure 8 illustrates that this assumption is not particularly crucial. In the worst case (at $\kappa_{pDNA} = 160\,\%$), pDNA production needs to be maintained for 8.3 h to perform at least as well as a non-starved process. Our experimental data (Figure 5 and 7) demonstrate

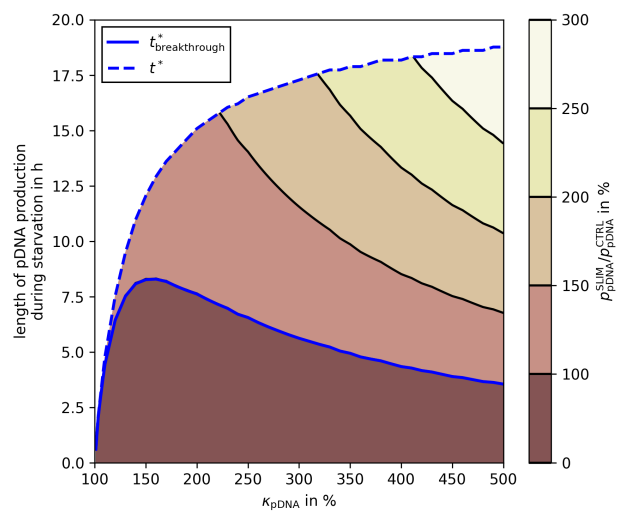

Figure 8: Breakthrough production length during starvation in linear fed-batch processes. If the pDNA production during starvation can be held longer than the breakthrough production length ($t^*_{breakthrough}$, blue full line), the SO_4^{2-} limited process outperforms a control (i.e., not starved) process. A visual explanation of $t^*_{breakthrough}$ is given in Figure S4. The start of the starvation is defined by the optimal $C_{SO_4^{2-}}(0)$ calculated in Figure 4A (red dotted line). The maximum pDNA production length during starvation is equal to the total starvation length t^* (blue dashed line). The contour colors indicate the productivity of a SO_4^{2-} limited process compared to the control in % (color bar on the right).

Table 2: Comparison of pDNA specific yields and volumetric yields in published studies. The last two rows show the results of the experiments of this study (all pDNA conformations). Values marked with † are estimated from published figures. Values marked with ‡ are calculated from reported values. Values marked with ⋆ are converted from OD_{600} to cell dry mass (0.33 $g/L/OD_{600}$, BNID109838 [53]). Values marked with § are estimated with 50 % GC content and an *E. coli* cell mass of 110 fg (BNID100498 [53]). Values reported as NA were not accessible.

Reference	yield		avg. vol. productivity	copy number	biomass conc.	pDNA length	origin of replication	selection pressure	*E. coli* strain	process type
	specific [$mg\,g^{-1}$]	volumetric [$mg\,L^{-1}$]	[$mg\,L^{-1}\,h^{-1}$]	[plasmid $cell^{-1}$]	[$g\,L^{-1}$]	[kbp]				
[54]	10.8‡	58.3	3.9	NA	5.4	NA	NA	ampicillin	BL21	shake flask
[11]	15 †⋆	57 †	8.2†‡	298§	3.8‡	5.4	pUC	ampicillin	DH5α	shake flask
[13]	2.4†	8.0	0.8‡	86§	3.3‡	3.0	pUC	kanamycin	BL21 *recA*-	batch
[55]	2.4	19.9	0.3	42§	8.3‡	6.1	pUC	ampicillin	VH34	batch
[56]	2.4	30.0	2.7†‡	42§	12.5‡	6.1	pUC	ampicillin	VH33	batch
[19]	7.0	230	17.7	192§	34	3.9	pUC	kanamycin	DH5α	batch
[20]	7.9	35.9	2.3‡	529§	4.6†	1.6	pUC	ampicillin	DH5α	batch
[57]	11.3	39.4	1.1†‡	176§	3.5†	6.9	pUC	ampicillin	DH5α	batch
[17]	17.1‡	60	0.7‡	286§	3.5	6.4	ColE1	none	JM109	batch
[16]	19.1	141	NA	553§	7.4‡	3.7	pUC	kanamycin	GALG20	batch
[18]	32.4	102.8	NA	526§	3.2	6.6	pBR322	ampicillin	VH33	batch
[10]	6.9‡	NA	NA	107§	NA	6.9	pUC	ampicillin	W3110	continuous
[58]	1.6	33	3.0	43§	20.6‡	4.0	pUC	none	DH5α	exp. fed-perfusion
[59]	10.1	74.8	3.1‡	451§	8.3	2.4	pUC	kanamycin	PFC	fed-batch in shake flask
[12]	1.2	50	4.1	21§	41	6.1	pUC	ampicillin	VH33	exp. fed-batch
[60]	7.6	25.6	NA	118§	3.4‡	6.9	pUC	ampicillin	DH5α	exp. fed-batch
[57]	9.1	44	1.3‡	141§	4.8‡	6.9	pUC	ampicillin	DH5α	exp./lin. fed-batch
[61]	9.5⋆	250	11.3†‡	217§	26.4⋆	4.7	f1	kanamycin	DH5α	lin. fed-batch
[62]	9.8	140	3.9†‡	284§	14.3‡	3.7	ColE1	kanamycin	GALG20	exp. fed-batch
[63]	31.2⋆	1923	72.4‡	NA	62 ‡⋆	NA	pUC	ampicillin	BL21 *recA*$^-$	lin. fed-batch
[64]	15.5	759	31.2	426§	49 ‡	3.9	pUC	kanamycin	DH5α	exp. fed-batch
[8]	25.9	939	35.1	1142	36 ‡	3.5	ColE1	none	JM108*murselect*	exp. fed-batch
[62]	55.8†‡⋆	2177	41 †‡	965§	39 †⋆	6.2	ColE1	kanamycin	GALG20	exp. fed-batch
[24]	51	2200	NA	841§	43 ‡	6.5	pUC	kanamycin	DH5α	exp. fed-batch
[65]	65 ⋆	1830	42 †‡	1659§	28 ‡⋆	4.2	pUC	none	NTC4862	exp. fed-batch
[25]	68 ⋆	2590	NA	1176§	38 ‡⋆	6.2	pUC	kanamycin	DH5α	exp. fed-batch
control	57.1±0.7	2528 ±68	81.5±2.2	510§	44.2±0.9	12.0	pUC	none	JM108	lin. fed-batch
SO_4^{2-} limited	73.9±4.6	2788 ±161	89.9±5.2	660§	38.2±1.0	12.0	pUC	none	JM108	lin. fed-batch

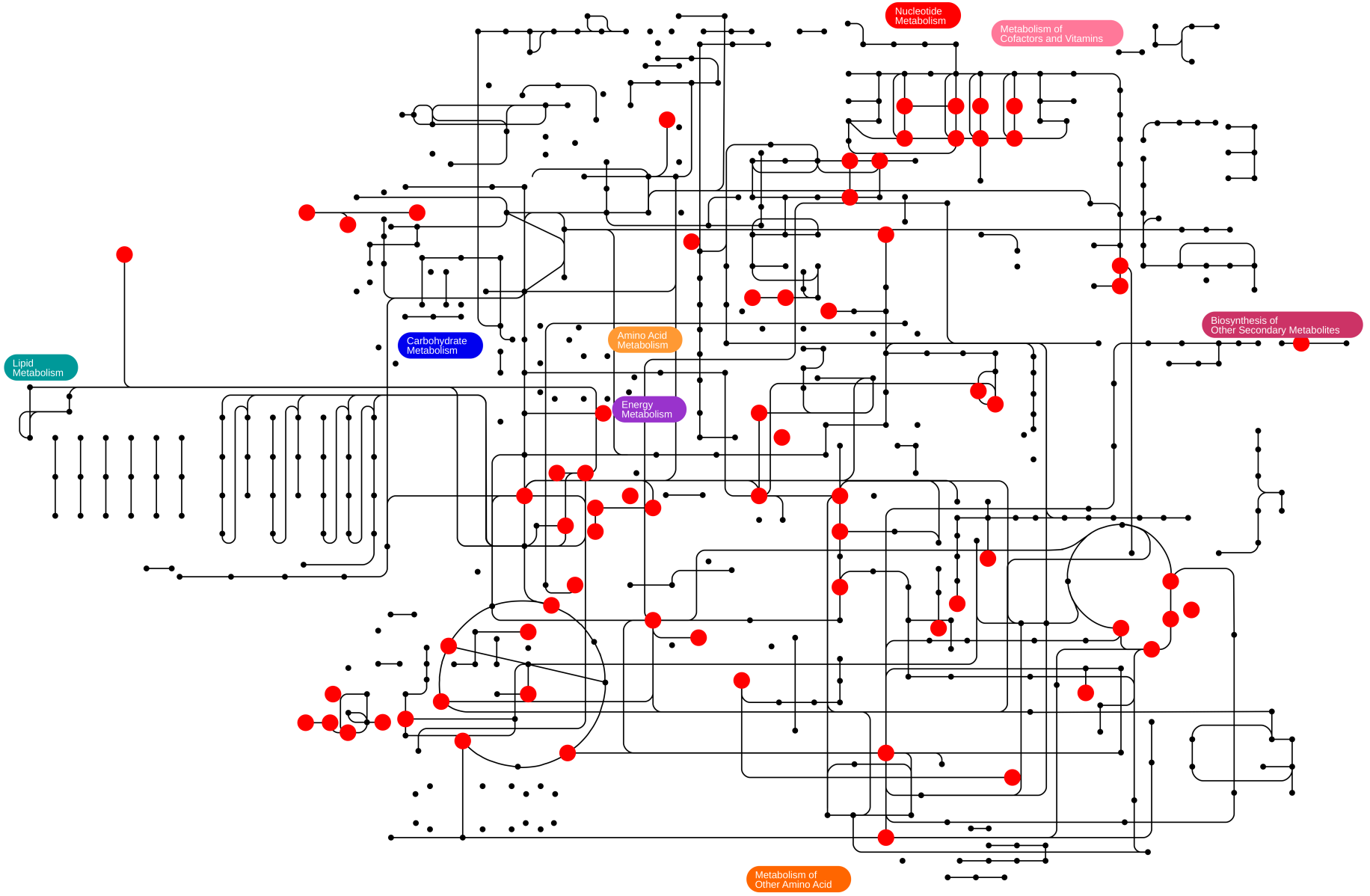

Figure 9: **Applicability of sulfate limitation to other biotechnologcial products.** Dots and lines indicate metabolites and reactions, respectively, annotated in *i*ML1515. Metabolites shown as red circles are targets for productivity improvement by sulfate limitation. The figure was created with iPath 3.0 [66]. An interactive version of the map is available at `https://pathways.embl.de/selection/DfMG1nmoIuPIvOcdQSt`. A full list of identified targets is shown in Table S4.

that this is indeed feasible. Interestingly, if κ_{pDNA} is raised beyond 160 %, the optimal starvation time increases too, but the minimally required length of pDNA production during starvation drops. This hints at a possible trade-off that may be explored in further process optimization steps.

In a growth-decoupled process, it is essential to, first, reach high biomass which can subsequently catalyze product formation. With our process settings (i.e., fixed final process volume), this is best achieved with a linear feeding regime (Figure S2), which quickly builds up biomass during the first few hours (compare Figure S2B and E).

We experimentally verified that a linear feeding strategy (which results in a continuously decreasing growth rate) outperforms the exponential feed even without sulfate limitation (data not shown). This is in agreement with literature which shows that a lower growth rate is preferential for pDNA production [10–12]. Interestingly a literature survey (Table 2) reveals that exponential feeding strategies are more frequently used which may explain why even our linear control process is able to outperform the majority of previously reported values. However, an ultimate comparison cannot be made as these studies used different plasmids which may significantly influence the evaluation metrics of the production process [21].

A key challenge in any growth-decoupled process is to maintain metabolic activity in non-growing metabolic states. Often a strong decrease in nutrient uptake is observed [43]. However, during sulfate starvation, glucose concentration in the reactor remained below the detection limit, indicating that cells consistently maintained glucose uptake equal to the glucose feed rate. This supports the validity of our assumption stated in Equation 5. We speculate that this may be related to the fact that (i) due to the linear feed, the specific glucose uptake already dropped to 4 % of its initial value at the onset of starvation – 81 % lower than the (already) reduced specific glucose uptake rate during sulfate starvation reported by Masuda et al. [43]; (ii) sulfate starvation retains high ATP-levels compared to other nutrient limitations [45, 67].

Consistent with maintained metabolic activity, we detected acetate accumulation during starvation (Figure S5), which is a common sign of overflow metabolism in *E. coli* [68]. However, our theoretical predictions for the maximum acetate concentration exceeded the measured values, suggesting the existence of other byproducts. Identifying these will be the focus of future research.

In the future, additional refinement of the process model could be achieved by including a term for the metabolic burden of resistance protein synthesis. An appropriate computational framework has recently been published [69]. Several studies have shown that this may significantly influence the metabolism of a producing organism [7, 8].

In both control and SO_4^{2-} limited experiments, specific pDNA yields and concentrations dropped at the end of the bioprocess. This might be due to other limitations (e.g., the O_2 transfer rate [70]). Therefore, we suggest stopping the process at 31 h. At that point product concentration, average volumetric productivity, and specific yield are statistically significantly up by 10 %, 10 %, and 29 %, respectively (compared to control). Considering the fraction of supercoiled pDNA, the sulfate limited process gains another 3 % points to concentration and productivity, and 4 % points to specific yield. A mechanistic interpretation of this interesting observation, however, is outside the scope of the current methodology and will be the focus of further work.

Despite using a defined, minimal medium and a comparatively large plasmid (12 kbp) our process outperforms previous reports [25] achieving an 8 % increase in volumetric yield and a 9 % boost in specific yield (Table 2). The latter is not only advantageous for higher pDNA quantities in sulfate limited experiments but, importantly, also aids in downstream processing [71, 72].

To showcase the broad applicability of sulfate limitation in biotechnological production, we explored the effect of sulfate limitation on 307 naturally secreted products of *E. coli* that are listed in the *i*ML1515 model [29]. Through lexicographic FBA with and without sulfate in the medium, we identified 83 compounds – more than 25 % of those investigated – that would benefit from sulfate limitation in their production (Figure 9). This underscores the significant potential of sulfate limited process design for a wide range of biotechnological products.

5. Conclusion

Based on genome-scale metabolic modeling, we have designed and successfully validated a three-stage, growth-decoupled fed-batch process for pDNA production in *E. coli*, cultivated in a minimal medium. We achieved the transition between the growth and production phases through sulfate starvation. This optimization led to statistically significant increases in key metrics: average supercoiled volumetric

productivity (+13 %), specific pDNA yield (+29 %), and supercoiled specific pDNA yield (+33 %). Overall, our process achieved a specific pDNA yield of 74 mg g^{-1} and a volumetric yield of 8 g L^{-1}, marking an increase of more than 8 % compared to prior reports. Importantly, our process design may be benefitial to a wide range of bio-based products of industrial significance.

Ethics Approval and Consent to Participate

Not applicable.

Consent for Publication

Not applicable.

Availablility of Data and Materials

All scripts and data are available at `https://github.com/Gotsmy/slim`.

Funding

MG and JZ received funding from enGenes Biotech GmbH and Baxalta Innovations GmbH, a part of Takeda companies.

Acknowledgements

Not applicable.

Authors' Information

[a] Department of Analytical Chemistry, University of Vienna, Vienna, 1090, Austria. [b] Doctorate School of Chemistry, University of Vienna, Vienna, 1090, Austria. [c] enGenes Biotech GmbH, Vienna, 1190, Austria. [d] Baxalta Innovations GmbH, A Part of Takeda Companies, Orth an der Donau, 2304, Austria.

Declaration of Interest

FS and FW are employees of enGenes Biotech GmbH. JM is co-founder and Chief Executive Officer of enGenes Biotech GmbH. PG and BK are employees of Baxalta Innovation GmbH. Employees of Baxalta Innovations GmbH may be owners of stock and/or stock options. MG, JZ, FS, FW, and JM are authors of a patent application that has been filed on the basis of the reported results.

CRediT authorship contribution statement

Mathias Gotsmy: Conceptualization, Methodology, Software, Formal Analysis, Investigation, Visualization, Writing – original draft, review and editing. **Florian Strobl:** Methodology, Formal Analysis, Investigation, Writing – review and editing. **Florian Weiß:** Methodology, Formal Analysis, Investigation, Writing – review and editing. **Petra Gruber:** Funding, Writing – review and editing. **Barbara Kraus:** Funding, Writing – review and editing. **Juergen Mairhofer:** Funding, Writing – review and editing. **Jürgen Zanghellini:** Conceptualization, Funding, Writing – original draft, review and editing.

References

[1] J. Mairhofer, A. R. Lara, Advances in host and vector development for the production of plasmid dna vaccines, in: Cancer Vaccines, Springer, 2014, pp. 505–541.

[2] European Medicines Agency, Comirnaty assessment report, `https://www.ema.europa.eu/en/documents/assessment-report/comirnaty-epar-public-assessment-report_en.pdf`, 2020. [Online; accessed 28-July-2022].

[3] A. Schmidt, H. Helgers, F. L. Vetter, A. Juckers, J. Strube, Fast and flexible mrna vaccine manufacturing as a solution to pandemic situations by adopting chemical engineering good practice—continuous autonomous operation in stainless steel equipment concepts, Processes 9 (2021) 1874.

[4] M. Ramamoorth, A. Narvekar, Non viral vectors in gene therapy-an overview, Journal of clinical and diagnostic research: JCDR 9 (2015) GE01.

[5] J.-Y. Cherng, N. Schuurmans-Nieuwenbroek, W. Jiskoot, H. Talsma, N. Zuidam, W. Hennink, D. Crommelin, Effect of dna topology on the transfection efficiency of poly ((2-dimethylamino) ethyl methacrylate)–plasmid complexes, Journal of controlled release 60 (1999) 343–353.

[6] L. Cupillard, V. Juillard, S. Latour, G. Colombet, N. Cachet, S. Richard, S. Blanchard, L. Fischer, Impact of plasmid supercoiling on the efficacy of a rabies dna vaccine to protect cats, Vaccine 23 (2005) 1910–1916.

[7] D. S. Cunningham, R. R. Koepsel, M. M. Ataai, M. M. Domach, Factors affecting plasmid production in escherichia coli from a resource allocation standpoint, Microbial cell factories 8 (2009) 1–17.

[8] J. Mairhofer, M. Cserjan-Puschmann, G. Striedner, K. Nöbauer, E. Razzazi-Fazeli, R. Grabherr, Marker-free plasmids for gene therapeutic applications—lack of antibiotic resistance gene substantially improves the manufacturing process, Journal of biotechnology 146 (2010) 130–137.

[9] D. M. Bower, K. L. Prather, Engineering of bacterial strains and vectors for the production of plasmid dna, Applied microbiology and biotechnology 82 (2009) 805–813.

[10] M. Wunderlich, H. Taymaz-Nikerel, G. Gosset, O. T. Ramírez, A. R. Lara, Effect of growth rate on plasmid dna production and metabolic

performance of engineered escherichia coli strains, Journal of bioscience and bioengineering 117 (2014) 336–342.

[11] J. Galindo, B. L. Barrón, A. R. Lara, Improved production of large plasmid dna by enzyme-controlled glucose release, Annals of Microbiology 66 (2016) 1337–1342.

[12] R. Soto, L. Caspeta, B. Barrón, G. Gosset, O. T. Ramírez, A. R. Lara, High cell-density cultivation in batch mode for plasmid dna production by a metabolically engineered e. coli strain with minimized overflow metabolism, Biochemical engineering journal 56 (2011) 165–171.

[13] K. E. Jaén, D. Velazquez, F. Delvigne, J.-C. Sigala, A. R. Lara, Engineering e. coli for improved microaerobic pdna production, Bioprocess and biosystems engineering 42 (2019) 1457–1466.

[14] A. R. Lara, K. E. Jaén, O. Folarin, E. Keshavarz-Moore, J. Büchs, Effect of the oxygen transfer rate on oxygen-limited production of plasmid dna by escherichia coli, Biochemical Engineering Journal 150 (2019) 107303.

[15] D. S. Cunningham, Z. Liu, N. Domagalski, R. R. Koepsel, M. M. Ataai, M. M. Domach, Pyruvate kinase-deficient escherichia coli exhibits increased plasmid copy number and cyclic amp levels, Journal of bacteriology 191 (2009) 3041–3049.

[16] G. A. Gonçalves, D. M. Prazeres, G. A. Monteiro, K. L. Prather, De novo creation of mg1655-derived e. coli strains specifically designed for plasmid dna production, Applied microbiology and biotechnology 97 (2013) 611–620.

[17] Z. Wang, G. Le, Y. Shi, G. Wegrzyn, Medium design for plasmid dna production based on stoichiometric model, Process Biochemistry 36 (2001) 1085–1093.

[18] L. Martins, A. Pedro, D. Oppolzer, F. Sousa, J. Queiroz, L. Passarinha, Enhanced biosynthesis of plasmid dna from escherichia coli vh33 using box–behnken design associated to aromatic amino acids pathway, Biochemical Engineering Journal 98 (2015) 117–126.

[19] F. Islas-Lugo, J. Vega-Estrada, C. A. Alvis, J. Ortega-Lopez, M. del Carmen Montes-Horcasitas, Developing strategies to increase plasmid dna production in escherichia coli dh5α using batch culture, Journal of biotechnology 233 (2016) 66–73.

[20] M. K. Danquah, G. M. Forde, Growth medium selection and its economic impact on plasmid dna production, Journal of bioscience and bioengineering 104 (2007) 490–497.

[21] A. Kay, R. O'Kennedy, J. Ward, E. Keshavarz-Moore, Impact of plasmid size on cellular oxygen demand in escherichia coli, Biotechnology and applied biochemistry 38 (2003) 1–7.

[22] O. Folarin, D. Nesbeth, J. M. Ward, E. Keshavarz-Moore, Application of plasmid engineering to enhance yield and quality of plasmid for vaccine and gene therapy, Bioengineering 6 (2019) 54.

[23] K. E. Jaén, D. Velázquez, J.-C. Sigala, A. R. Lara, Design of a microaerobically inducible replicon for high-yield plasmid dna production, Biotechnology and Bioengineering 116 (2019) 2514–2525.

[24] J. A. Williams, J. Luke, S. Langtry, S. Anderson, C. P. Hodgson, A. E. Carnes, Generic plasmid dna production platform incorporating low metabolic burden seed-stock and fed-batch fermentation processes, Biotechnology and bioengineering 103 (2009) 1129–1143.

[25] A. E. Carnes, J. M. Luke, J. M. Vincent, A. Schukar, S. Anderson, C. P. Hodgson, J. A. Williams, Plasmid dna fermentation strain and process-specific effects on vector yield, quality, and transgene expression, Biotechnology and bioengineering 108 (2011) 354–363.

[26] K. E. Jaén, A. R. Lara, O. T. Ramírez, Effect of heating rate on pdna production by e. coli, Biochemical engineering journal 79 (2013) 230–238.

[27] G. Monteiro, S. Duarte, M. Martins, S. Andrade, D. Prazeres, High copy number plasmid engineering for biopharmaceutical-grade pdna production in lactococcus lactis, Journal of Biotechnology 305 (2019) S23–S24.

[28] S. O. Duarte, G. A. Monteiro, Plasmid replicons for the production of pharmaceutical-grade pdna, proteins and antigens by lactococcus lactis cell factories, International Journal of Molecular Sciences 22 (2021) 1379.

[29] J. M. Monk, C. J. Lloyd, E. Brunk, N. Mih, A. Sastry, Z. King, R. Takeuchi, W. Nomura, Z. Zhang, H. Mori, et al., i ml1515, a knowledgebase that computes escherichia coli traits, Nature biotechnology 35 (2017) 904–908.

[30] A. Ebrahim, J. A. Lerman, B. O. Palsson, D. R. Hyduke, Cobrapy: constraints-based reconstruction and analysis for python, BMC systems biology 7 (2013) 1–6.

[31] F. C. Neidhardt, J. L. Ingraham, M. Schaechter, Physiology of the bacterial cell; a molecular approach, 589.901 N397, Sinauer associates, 1990.

[32] Y. Sun, R. M. Fleming, I. Thiele, M. A. Saunders, Robust flux balance analysis of multiscale biochemical reaction networks, BMC bioinformatics 14 (2013) 1–6.

[33] N. E. Lewis, K. K. Hixson, T. M. Conrad, J. A. Lerman, P. Charusanti, A. D. Polpitiya, J. N. Adkins, G. Schramm, S. O. Purvine, D. Lopez-Ferrer, et al., Omic data from evolved e. coli are consistent with computed optimal growth from genome-scale models, Molecular systems biology 6 (2010) 390.

[34] R. Mahadevan, J. S. Edwards, F. J. Doyle III, Dynamic flux balance analysis of diauxic growth in escherichia coli, Biophysical journal 83 (2002) 1331–1340.

[35] K. Höffner, S. M. Harwood, P. I. Barton, A reliable simulator for dynamic flux balance analysis, Biotechnology and bioengineering 110 (2013) 792–802.

[36] P. Virtanen, R. Gommers, T. E. Oliphant, M. Haberland, T. Reddy, D. Cournapeau, E. Burovski, P. Peterson, W. Weckesser, J. Bright, et al., Scipy 1.0: fundamental algorithms for scientific computing in python, Nature methods 17 (2020) 261–272.

[37] C. Yanisch-Perron, J. Vieira, J. Messing, Improved m13 phage cloning vectors and host strains: nucleotide sequences of the m13mpl8 and puc19 vectors, Gene 33 (1985) 103–119.

[38] H. C. Bimboim, J. Doly, A rapid alkaline extraction procedure for screening recombinant plasmid dna, Nucleic acids research 7 (1979) 1513–1523.

[39] B. Dahlgren, O. Čertík, finitediff, 2021. URL: https://github.com/bjodah/finitediff. doi:https://dx.doi.org/10.5281/zenodo.5168369.

[40] B. Fornberg, Classroom note: Calculation of weights in finite difference formulas, SIAM review 40 (1998) 685–691.

[41] H. C. Lange, J. J. Heijnen, Statistical reconciliation of the elemental and molecular biomass composition of Saccharomyces cerevisiae, Biotechnology and Bioengineering 75 (2001) 334–344.

[42] S. Klamt, R. Mahadevan, O. Hädicke, When do two-stage processes outperform one-stage processes?, Biotechnology journal 13 (2018) 1700539.

[43] A. Masuda, Y. Toya, H. Shimizu, Metabolic impact of nutrient starvation in mevalonate-producing escherichia coli, Bioresource technology 245 (2017) 1634–1640.

[44] C. Willrodt, A. Hoschek, B. Bühler, A. Schmid, M. K. Julsing, Decoupling production from growth by magnesium sulfate limitation boosts de novo limonene production, Biotechnology and Bioengineering 113 (2016) 1305–1314.

[45] K. Tokuyama, Y. Toya, F. Matsuda, B. F. Cress, M. A. Koffas, H. Shimizu, Magnesium starvation improves production of malonyl-coa-derived metabolites in escherichia coli, Metabolic engineering 52 (2019) 215–223.

[46] P. Stargardt, L. Feuchtenhofer, M. Cserjan-Puschmann, G. Striedner, J. Mairhofer, Bacteriophage inspired growth-decoupled recombinant protein production in escherichia coli, ACS Synthetic Biology 9 (2020) 1336–1348.

[47] C. J. Hartline, A. C. Schmitz, Y. Han, F. Zhang, Dynamic control in metabolic engineering: Theories, tools, and applications, Metabolic Engineering 63 (2021) 126–140.

[48] N. Venayak, A. von Kamp, S. Klamt, R. Mahadevan, MoVE identifies metabolic valves to switch between phenotypic states, Nature Communications 9 (2018) 5332.

[49] W. Maret, P. Blower, Teaching the chemical elements in biochemistry: Elemental biology and metallomics, Biochemistry and Molecular Biology Education 50 (2022) 283–289.

[50] N. R. C. U. C. o. D. a. Health, Trace Elements, in: Diet and Health: Implications for Reducing Chronic Disease Risk, National Academies Press (US), 1989, p. 301. URL: https://www.ncbi.nlm.nih.gov/books/NBK218751/.

[51] D. Markovich, Physiological roles and regulation of mammalian sulfate transporters, Physiological reviews 81 (2001) 1499–1533.

[52] A. St John, A. Goldberg, Effects of starvation for potassium and other inorganic ions on protein degradation and ribonucleic acid synthesis in escherichia coli, Journal of bacteriology 143 (1980) 1223–1233.

[53] R. Milo, P. Jorgensen, U. Moran, G. Weber, M. Springer, Bionumbers—the database of key numbers in molecular and cell biology, Nucleic acids research 38 (2010) D750–D753.

[54] Z.-N. Xu, W.-h. Shen, H. Chen, P.-l. Cen, Effects of medium composition on the production of plasmid dna vector potentially for human gene therapy, Journal of Zhejiang University. Science. B 6 (2005) 396.

[55] T. E. Pablos, R. Soto, E. M. Mora, S. Le Borgne, O. T. Ramírez, G. Gosset, A. R. Lara, Enhanced production of plasmid dna by engineered escherichia coli strains, Journal of biotechnology 158 (2012) 211–214.

[56] J. T. Cortés, N. Flores, F. Bolívar, A. R. Lara, O. T. Ramírez, Physiological effects of ph gradients on escherichia coli during plasmid dna production, Biotechnology and bioengineering 113 (2016) 598–611.

[57] A. Dorward, R. D. O'Kennedy, O. Folarin, J. M. Ward, E. Keshavarz-Moore, The role of amino acids in the amplification and quality of dna vectors for industrial applications, Biotechnology Progress 35 (2019) e2883.

[58] A. García-Rendón, R. Munguía-Soto, R. M. Montesinos-Cisneros, R. Guzman, A. Tejeda-Mansir, Performance analysis of exponential-fed perfusion cultures for pdna vaccines production, Journal of Chemical Technology & Biotechnology 92 (2017) 342–349.

[59] M. de la Cruz, E. A. Ramírez, J.-C. Sigala, J. Utrilla, A. R. Lara, Plasmid dna production in proteome-reduced escherichia coli, Microorganisms 8 (2020) 1444.

[60] R. D. O'Kennedy, J. M. Ward, E. Keshavarz-Moore, Effects of fermentation strategy on the characteristics of plasmid dna production, Biotechnology and applied biochemistry 37 (2003) 83–90.

[61] K. O'Mahony, R. Freitag, F. Hilbrig, P. Müller, I. Schumacher, Strategies for high titre plasmid dna production in escherichia coli dh5α, Process Biochemistry 42 (2007) 1039–1049.

[62] G. A. Goncalves, K. L. Prather, G. A. Monteiro, A. E. Carnes, D. M. Prazeres, Plasmid dna production with escherichia coli galg20, a pgi-gene knockout strain: Fermentation strategies and impact on downstream processing, Journal of biotechnology 186 (2014) 119–127.

[63] J.-N. Phue, S. J. Lee, L. Trinh, J. Shiloach, Modified escherichia coli b (bl21), a superior producer of plasmid dna compared with escherichia coli k (dh5α), Biotechnology and bioengineering 101 (2008) 831–836.

[64] F. Grijalva-Hernández, J. Vega-Estrada, M. Escobar-Rosales, J. Ortega-López, R. Aguilar-López, A. R. Lara, M. d. C. Montes-Horcasitas, High kanamycin concentration as another stress factor additional to temperature to increase pdna production in e. coli dh5α batch and fed-batch cultures, Microorganisms 7 (2019) 711.

[65] J. Nelson, S. Rodriguez, N. Finlayson, J. Williams, A. Carnes, Antibiotic-free production of a herpes simplex virus 2 dna vaccine in a high yield cgmp process, Human Vaccines & Immunotherapeutics 9 (2013) 2211–2215.

[66] Y. Darzi, I. Letunic, P. Bork, T. Yamada, ipath3. 0: interactive pathways explorer v3, Nucleic acids research 46 (2018) W510–W513.

[67] V. Chubukov, U. Sauer, Environmental dependence of stationary-phase metabolism in bacillus subtilis and escherichia coli, Applied and environmental microbiology 80 (2014) 2901–2909.

[68] E. El-Mansi, W. Holms, Control of carbon flux to acetate excretion during growth of escherichia coli in batch and continuous cultures, Microbiology 135 (1989) 2875–2883.

[69] O. Oftadeh, V. Hatzimanikatis, Application of genome-scale models of metabolism and expression to the simulation and design of recombinant organisms, bioRxiv (2023) 2023–09.

[70] A. Castan, S.-O. Enfors, Characteristics of a do-controlled fed-batch culture of escherichia coli, Bioprocess Engineering 22 (2000) 509–515.

[71] K. J. Prather, S. Sagar, J. Murphy, M. Chartrain, Industrial scale production of plasmid dna for vaccine and gene therapy: plasmid design, production, and purification, Enzyme and microbial technology 33 (2003) 865–883.

[72] J. A. Williams, A. E. Carnes, C. P. Hodgson, Plasmid dna vaccine vector design: impact on efficacy, safety and upstream production, Biotechnology advances 27 (2009) 353–370.

[73] P. Wong, S. Gladney, J. D. Keasling, Mathematical model of the lac operon: inducer exclusion, catabolite repression, and diauxic growth on glucose and lactose, Biotechnology progress 13 (1997) 132–143.

[74] A. Varma, B. O. Palsson, Stoichiometric flux balance models quantitatively predict growth and metabolic by-product secretion in wild-type escherichia coli w3110, Applied and environmental microbiology 60 (1994) 3724–3731.

[75] Z. A. King, J. Lu, A. Dräger, P. Miller, S. Federowicz, J. A. Lerman, A. Ebrahim, B. O. Palsson, N. E. Lewis, Bigg models: A platform for integrating, standardizing and sharing genome-scale models, Nucleic acids research 44 (2016) D515–D522.